



Investigation of chemical bath deposition of CdO thin films using three different complexing agents

Hani Khallaf^a, Chia-Ta Chen^{b,c}, Liann-Be Chang^{b,c},
Oleg Lupan^{a,d}, Aniruddha Dutta^{a,e}, Helge Heinrich^{a,e}, A. Shenouda^f, Lee Chow^{a,e,*}

^a Department of Physics, University of Central Florida, Orlando, FL 32816, USA

^b Graduate Institute of Electro-Optical Engineering, Chang Gung University, Kweishan, Taoyuan 333, Taiwan

^c Green Technology Research Center, Chang Gung University, Kweishan, Taoyuan 333, Taiwan

^d Department of Microelectronics and Semiconductor Devices, Technical University of Moldova, 168 Stefan cel Mare Boulevard, MD-2004 Chisinau, Republic of Moldova

^e Advanced Materials Processing and Analysis Centre, Department of Mechanical, Materials, and Aerospace Engineering, University of Central Florida, Orlando, FL 32816, USA

^f Central Metallurgical R&D Institute (CMRDI), Tebbin, P.O. Box 87, Helwan, Egypt

ARTICLE INFO

Article history:

Received 6 March 2011

Accepted 12 April 2011

Available online 12 June 2011

Keywords:

CdO

Thin films

Group II–VI Semiconductors

Chemical bath deposition

ABSTRACT

Chemical bath deposition of CdO thin films using three different complexing agents, namely ammonia, ethanolamine, and methylamine is investigated. CdSO₄ is used as Cd precursor, while H₂O₂ is used as an oxidation agent. As-grown films are mainly cubic CdO₂, with some Cd(OH)₂ as well as CdO phases being detected. Annealing at 400 °C in air for 1 h transforms films into cubic CdO. The calculated optical band gap of as-grown films is in the range of 3.37–4.64 eV. Annealed films have a band gap of about 2.53 eV. Rutherford backscattering spectroscopy of as-grown films reveals cadmium to oxygen ratio of 1.00:1.74 ± 0.01 while much better stoichiometry is obtained after annealing, in accordance with the X-ray diffraction results. A carrier density as high as 1.89 × 10²⁰ cm⁻³ and a resistivity as low as 1.04 × 10⁻² Ω-cm are obtained.

© 2011 Elsevier B.V. All rights reserved.

1. Introduction

Chemical bath deposition (CBD) is the analog in liquid phase of the well-known chemical vapor deposition technique in the vapor phase. Among all techniques used to grow group II–VI semiconductors, CBD has the advantage of being a simple, low temperature, and inexpensive large-area deposition technique. It has been widely employed in the deposition of semiconductor thin films for over forty years [1]. CBD has been extensively used in growing group II–VI semiconductors, such as CdS [1–6], CdSe [7–10], HgS [11,12], HgSe [13,14], ZnS [15–18], ZnSe [19–22], and ZnO [23–26].

CdO thin films reported in the literature have been obtained mainly by dc magnetron reactive sputtering [27], metal organic chemical vapor deposition [28,29], vacuum evaporation [30], electrochemical deposition [31], pulsed laser deposition [32], electron beam evaporation [33], spray pyrolysis [34], sol–gel [35], RF magnetron sputtering [36], and successive ionic layer adsorption and reaction [37]. However, only few attempts to grow CdO thin films using CBD have been reported [38,39]. In both cases, only ammonia has been used as the complexing agent.

In this work, we report CBD of CdO thin films using three different complexing agents, namely ammonia, ethanolamine (EA), and methylamine (MA). Transmittance, reflectance measurements and band gap calculations are carried out for as-grown films as well as annealed films. Resistivity, carrier density, and Hall mobility of annealed films are acquired using Hall effect measurements. Crystal structure as well as crystal quality are examined using X-ray diffraction (XRD), transmission electron microscopy (TEM), and Fourier transform infrared spectroscopy (FTIR). Film morphology, composition, and binding energy are studied using scanning electron microscopy (SEM), Rutherford backscattering spectroscopy (RBS), and X-ray photoelectron spectroscopy (XPS), respectively.

2. Experimental details

CdO films were prepared using aqueous solutions of CdSO₄ (0.038 M), (NH₄)₂SO₄ (0.076 M), H₂O₂ (34%), and NH₄OH (29.4%). Each bath contained 100–120 ml of de-ionized water (resistivity ~18.2 MΩ-cm) that was kept under stirring at 85 °C. In addition to ammonia, two other complexing agents were used; EA and MA. To ensure the stability of Cd[NH₃]₄²⁺ complex in the main solution, ammonia was added whenever EA or MA is being used. Similar to our previous work on CBD-ZnO [23]. It was noticed that adding ammonia is necessary to dissolve the Cd(OH)₂ formed upon mixing the Cd-source and EA or MA. CdSO₄, (NH₄)₂SO₄, and the desired

* Corresponding author at: Department of Physics, University of Central Florida, 4000 Central Florida Blvd., Orlando, FL 32816, USA.

E-mail address: Lee.Chow@ucf.edu (L. Chow).

complexing agent were mixed at room temperature before being added to the main solution. Appropriate amounts of hydrogen peroxide were then added to the main solution. Films were grown on 38 mm × 38 mm × 1 mm glass substrates (Schott Borofloat glass). With the help of a Teflon holder, the glass substrate was kept vertically in the solution. All substrates were held in the bath prior to the addition of any of the reagents. To ensure deposition of high-quality, adhesive, and specularly reflecting films, the substrate was removed from the solution whenever the solution becomes turbid and the homogeneous reaction starts to take place. The cleaning steps of the substrate are reported elsewhere [4]. Specular transmittance measurements were carried out at room temperature in the wavelength range from 200 to 1200 nm, using a Cary 500 (Varian) double beam UV/VIS spectrophotometer. Specular reflectance measurements were performed at an angle of incidence of 7° in the same wavelength range. The optical absorption coefficient α was calculated for each film using the equation [40]:

$$T = (1 - R)^2 \exp(-\alpha t) \quad (1)$$

where T is transmittance, R is reflectance, and t is film thickness.

The absorption coefficient α is related to the incident photon energy $h\nu$ as:

$$\alpha = \frac{K(h\nu - E_g)^{n/2}}{h\nu} \quad (2)$$

where K is a constant, E_g is the optical band gap, and n is equal to 1 for direct band gap material such as CdO. The band gap was determined for each film by plotting $(\alpha h\nu)^2$ versus $h\nu$ and then extrapolating the straight line portion to the energy axis. Resistivity, Hall mobility, and carrier density were evaluated by Hall effect measurements at room temperature in a Van der Pauw four-point probe configuration, using indium contacts, in an automated Hall effect system (Ecopia HMS-3000, Bridge Technology, Chandler Heights AZ, USA) with a 0.55 T magnetic induction. XRD was carried out using Rigaku D XRD unit (with 40 kV, 30 mA CuK α radiation, $\lambda = 0.15406$ nm). The sample was mounted at 2.5° and scanned from 25° to 80° in steps of 0.02° with a scan rate of 1.2° min⁻¹. Transmission electron microscopy was performed using a Tecnai F30 TEM system operating at an acceleration voltage of 300 kV. Cross sections of CdO films were prepared with FEI 200 focused ion beam system. SEM micrographs were obtained using a JEOL 6400F SEM at an acceleration voltage of 10 kV. The FTIR micro-analysis was performed at room temperature using contact ATR optimized objective that covers a range of wavenumbers from 650 cm⁻¹ to 4000 cm⁻¹. RBS measurements were acquired using a 2.25 MeV α -particles IONIX 1.7 MU Tandemtron, with a surface barrier detector with energy resolution ≤ 15 keV (full width at half maximum-FWHM),

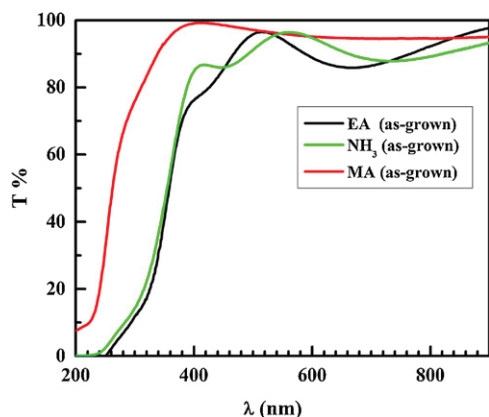


Fig. 1. Specular transmittance of as-grown films deposited using three different complexing agents.

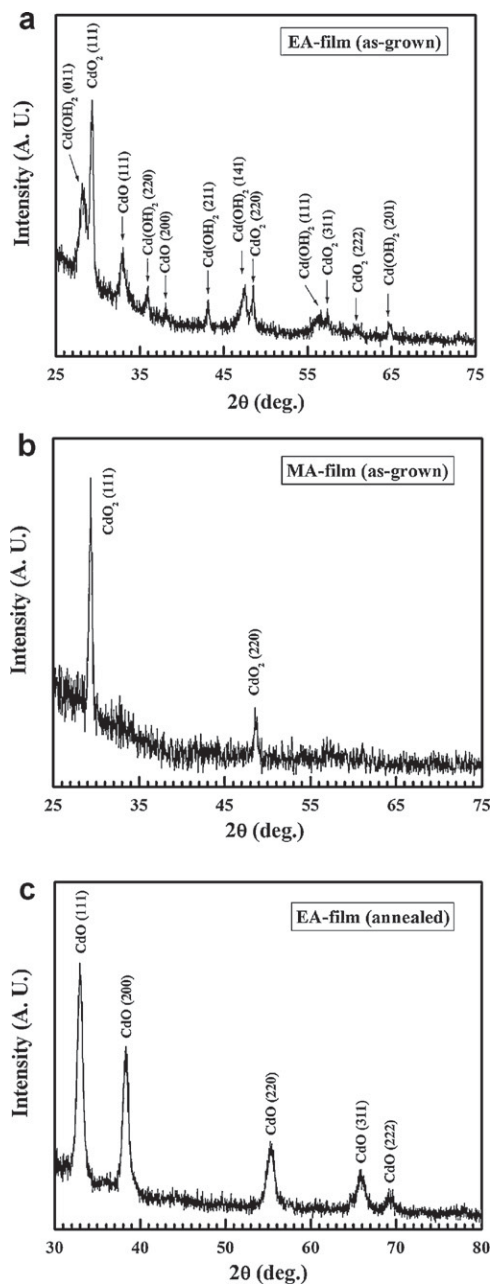


Fig. 2. XRD pattern of (a) as-grown EA-based film, (b) as-grown MA-based film, and (c) annealed EA-based film.

positioned at a scattering angle of 165°. XPS was performed on a Physical Electronics PHI 5400 ESCA using unmonochromated Mg K α radiation at 1253.6 eV. Each of the XPS spectra was acquired from 30 repeated sweeps. XPS spectra were corrected from charging effects by referencing the adventitious C 1s peak to 284.6 eV.

3. Results and discussion

Fig. 1 shows the optical transmittance of as-grown films for all three complexing agents. As shown, all three films exhibit high transmittance that exceeds 80% in the visible region. The NH₃-based and EA-based films exhibit a sharp absorption edge around 365–370 nm, while the absorption edge of the MA-based film is around 270 nm. Such high transmittance and sharp absorption edge observed indicate the high quality of all three films. The calculated band gap is 3.37 eV, 3.40 eV, and 4.64 eV for the EA-based, NH₃-

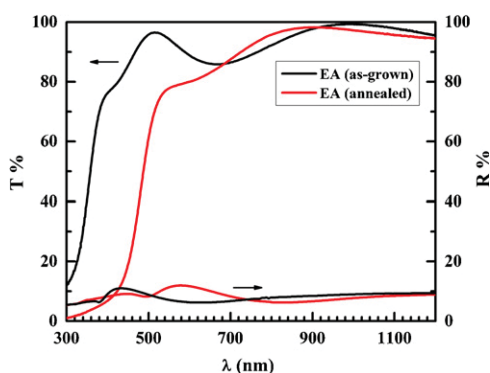


Fig. 3. Specular transmittance and reflectance of as-grown and annealed EA-based film.

based, and MA-based films, respectively. The blue shift observed in the case of MA-based films can be understood by comparing its XRD pattern to that of EA-based film. According to Fig. 2(a), the as-grown EA-based film consists of a mixture of three different phases; cubic CdO [41], monoclinic/hexagonal Cd(OH)₂ [42,43], and cubic CdO₂ [44]. However, as shown in Fig. 2(b), only cubic phase of CdO₂ is detected for as-grown MA-film. It should be noted that the XRD pattern of as-grown NH₃-film (not shown in this work) is similar to that of EA-based film. This may explain why both films almost share the same absorption edge, while a blue shift of more than 1.2 eV is observed in the case of MA-based film. After annealing at 400 °C in air for 1 h, all three films are fully transformed into CdO. Fig. 2(c) shows the XRD pattern of annealed EA-based film, with only cubic phase of CdO [45] being detected. Similar XRD patterns are obtained for both MA-based and NH₃-based films annealed under the same conditions.

Such transformation to CdO after annealing is responsible for the red shift observed in the optical transmittance (Fig. 3) and the optical band gap (Fig. 4) of EA-based film. (For interpretation of the references to color in this text, the reader is referred to the web version of the article.) The band gap of annealed CdO films is 2.53 eV, which agrees with the 2.55 eV [38], 2.57 eV [46], and 2.58 eV [47] band gap values reported earlier in the literature for CdO.

FTIR absorption measurements shown in Fig. 5 agree with the XRD findings. Similar to what we have previously observed for CBD-ZnO [23], FTIR of as-grown EA-based film (Fig. 5(a)) detects a broadband around 3300 cm⁻¹ which is assigned to the O–H stretching mode of the hydroxyl group. This confirms the presence of the Cd(OH)₂ phase in as-grown EA-based films. This broadband disappears after annealing, as shown in Fig. 5(b). However, as shown in Fig. 5(c), such broadband does not exist in the case of

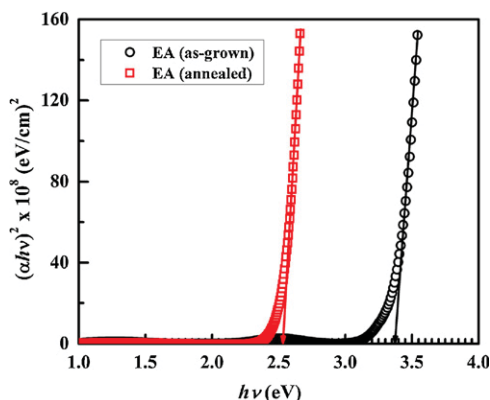


Fig. 4. Optical band gap calculations of as-grown and annealed EA-based film.

as-grown MA-based film. It should be noted that peaks detected between 2840 cm⁻¹ and 2930 cm⁻¹ (Fig. 5(a)) are due to the C–H stretching vibration mode, which corresponds to the CH₂ group of ethanolamine, which disappears after annealing as EA-based film is fully transformed into CdO. Absorbance peaks observed between 650 cm⁻¹ and 1500 cm⁻¹ are due to Si–O and B–O stretching vibrations [48] from the Borofloat glass substrate. It is worth noting that the boron content of Borofloat glass is about 5.2%.

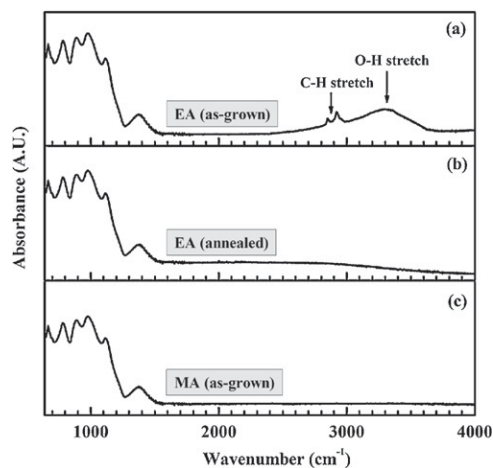


Fig. 5. FTIR absorbance spectrum of (a) as-grown EA-based film, (b) annealed EA-based film, and (c) as-grown MA-based film.

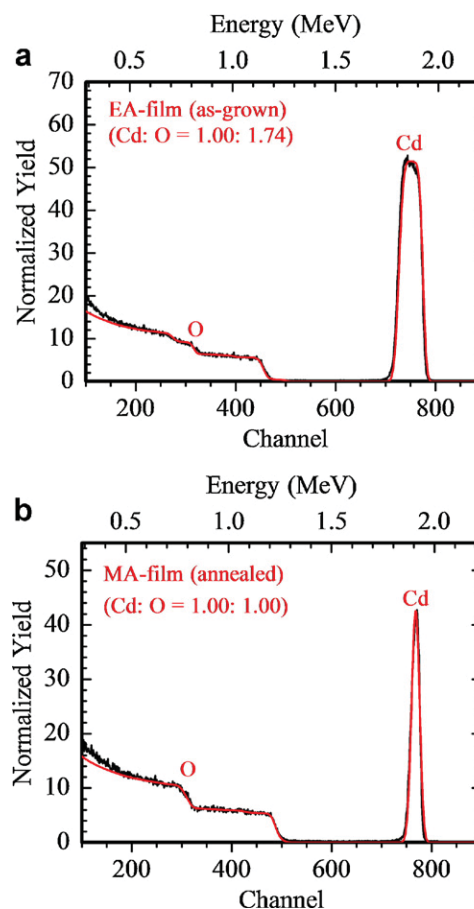


Fig. 6. RBS spectrum and RUMP simulation of (a) as-grown EA-based film and (b) annealed MA-based film.

Fig. 6(a) shows the RBS spectra of as-grown EA-based film. Simulation using Rutherford Universal Manipulation Program (RUMP) [49] was implemented to obtain the best possible match to the raw RBS spectra. As shown, the Cd:O ratio obtained for the as-grown film is $(1.00:1.74 \pm 0.01)$. This again confirms the presence of CdO, in addition to CdO₂ and Cd(OH)₂, in the as-grown EA-based films. Should the film contains only mixed phases of CdO₂ and Cd(OH)₂, a ratio of about $(1.00:2.00)$ will be observed. Such ratio is obtained in the case of as-grown MA-based film (not shown in this work). Fig. 6(b), however, shows the RBS spectra of MA-annealed film, where a ratio of $(1.00:1.00 \pm 0.01)$ is observed. This indeed confirms that, after annealing at 400 °C in air, films are fully transformed into CdO.

The XPS multiplex spectra of the Cd 3d_{5/2} and 3d_{3/2} peaks of as-grown as well as annealed EA-based films are shown in Fig. 7(a). As shown, Cd 3d_{5/2} and 3d_{3/2} peaks of the annealed film are symmetric and located at 405 eV and 411.8 eV which agrees well with the 6.74 eV spin-orbit energy splitting between Cd 3d_{5/2} and 3d_{3/2} states [50]. However, both peaks of as-grown film are asymmetric. As shown in Fig. 7(b), deconvolution of the Cd 3d_{5/2} peak renders three peaks with binding energies of 403.7 eV, 404.5 eV, and 405.4 eV. These three binding states can be assigned to CdO₂, Cd(OH)₂, and CdO, respectively [50]. This also confirms the XRD, FTIR, and RBS findings of the mixed phase nature of as-grown EA-based film. Similar deconvolution carried out for the Cd 3d_{3/2} peak is also shown in Fig. 7(b). All three peaks obtained maintain a ~6.7 eV energy difference from their corresponding Cd 3d_{5/2} peaks. Finally, it should be noted that both 405.4 eV and 405 eV values observed in as grown and annealed films lie within the accepted values of Cd 3d_{5/2} binding energies of CdO [50].

Fig. 8(a) shows the XPS multiplex spectra of the O 1s peak for as-grown and annealed EA-based films. Similar to the Cd 3d peaks, the O 1s peak of annealed film is symmetric while that of as-grown film is asymmetric. The O 1s binding energy of annealed film is located at 529.9 eV, which lies within the 527.7–530.6 eV range characteristic of O²⁻ oxides [50,51]. As shown in Fig. 8(b), a deconvolution of the O 1s peak of as-grown film renders two doublets

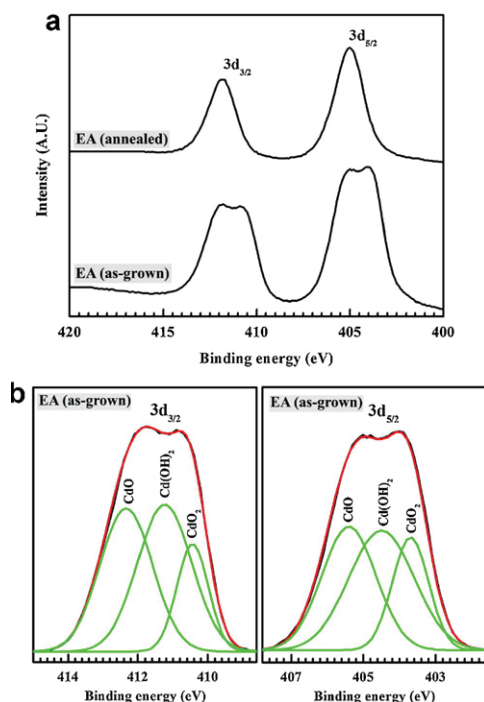


Fig. 7. (a) XPS multiplex spectra of Cd 3d of as-grown and annealed EA-based film and (b) deconvolution of the Cd 3d peaks of as-grown EA-based film.

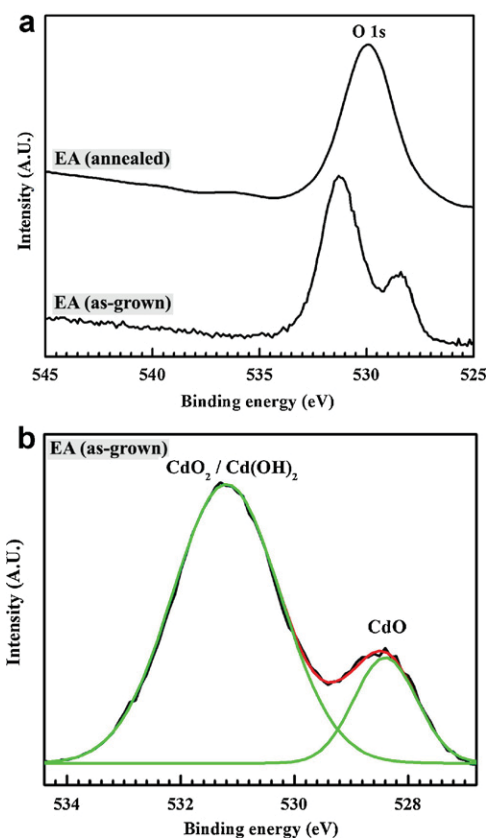


Fig. 8. (a) XPS multiplex spectra of O 1s of as-grown and annealed EA-based film and (b) deconvolution of the O 1s peak of as-grown EA-based film.

with the main doublet located at 531.1 eV and the smaller one located at 528.4 eV. According to Dupin et al. [51], binding energies in the range of 530.6–531.1 eV are characteristics of oxygen species integrated in the material as OH⁻ or O²⁻. Therefore, the main contribution observed at 531.1 eV is due to either cadmium peroxide or cadmium hydroxide, while the contribution at 528.4 eV is characteristic of cadmium oxide, which again agrees with the XRD, FTIR, and RBS findings of the mixed phase nature of as-grown EA-based film.

High-resolution transmission electron microscopy (HRTEM) image of annealed EA-based film is shown in Fig. 9. As shown, the CdO layer is about 0.25 μm. Only small variations in film thickness are observed. Occasional cracks due to annealing are found, as indicated by arrows near the edge of the film. The small area elec-

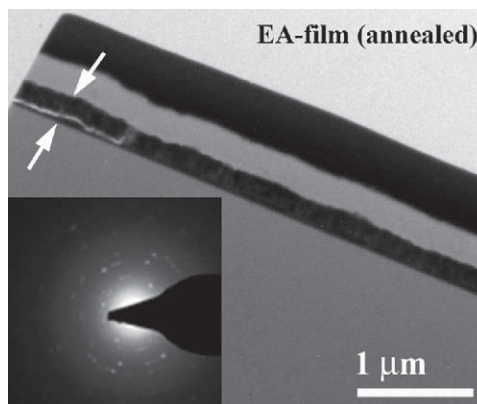


Fig. 9. HRTEM and SAED diffraction pattern (inset) of annealed EA-based CdO film.

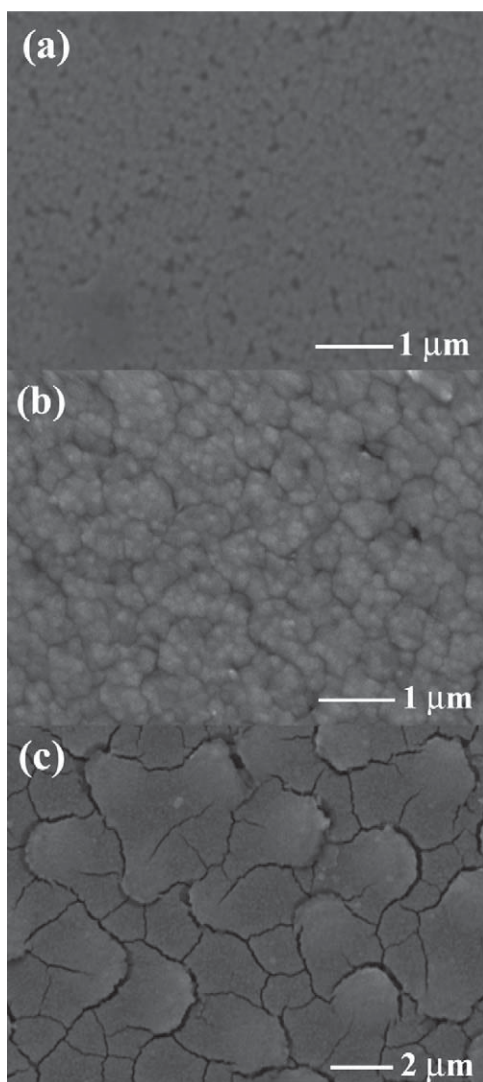


Fig. 10. SEM micrographs of (a) annealed MA-based film, (b) annealed EA-based film, and (c) annealed NH_3 -based film.

tron diffraction (SAED) pattern observed (inset of Fig. 9) confirms that CdO film is polycrystalline with a cubic crystal lattice. SEM micrographs of annealed MA, EA, and NH_3 -based films are shown in Fig. 10. As shown, MA and EA-based films maintain their integrity after annealing while NH_3 -based films deteriorate when annealed, as indicated by the high density of cracks shown in Fig. 10(c). This could be attributed to stress in as-grown NH_3 -based films, which caused films to lose their integrity after annealing. We have reported similar observations for EA-based ZnO films in a previous work [23]. Some pinholes have been observed in MA-based film (Fig. 10(a)). It is also noticed that, when compared to EA-film, average grain size of MA-film is much smaller. EA-based film, however, is continuous with much smoother surface than the other two films. This will have a significant impact on film resistivity and mobility as will be shown.

Table 1
Hall effect measurements of annealed EA, MA and NH_3 -based CdO films.

Sample	Carrier density (cm^{-3})	Mobility ($\text{cm}^2 \text{V}^{-1} \text{S}^{-1}$)	Resistivity ($\Omega\text{-cm}$)
EA-based	1.89×10^{20}	3.17×10^0	1.04×10^{-2}
MA-based	4.35×10^{18}	3.91×10^{-1}	3.67×10^0
NH_3 -based	7.55×10^{17}	8.21×10^{-1}	1.01×10^1

Table 1 summarizes the carrier density, resistivity, and Hall mobility of annealed EA, MA, and NH_3 -based films as revealed by Hall measurements carried out at room temperature. As shown, EA-films have the highest mobility and lowest resistivity among all three films. Resistivity of MA-films is two orders of magnitude higher, while that of NH_3 -films is three orders of magnitude higher than that of EA-films. Hall mobility of both films is also much smaller than that of EA-film. We believe that pinholes, small grain size, and high density of cracks observed under SEM (Fig. 10) are responsible for such drop in film resistivity and Hall mobility. High carrier density observed in EA-film can be attributed to oxygen deficiency in the film due to annealing. It is widely believed that excess Cd content in CdO films results in Cd ions occupying interstitial sites where they act as donors which, in turn, increases carrier density and lowers film resistivity.

SEM and Hall measurements suggest that EA-based CdO films are the best candidates for fabricating transparent conducting oxides using chemical bath deposition. These films are found to be of high quality, good uniformity, high transmittance, and good crystallinity. In addition, high conductivity is observed in EA-based films where a carrier density as high as $1.89 \times 10^{20} \text{ cm}^{-3}$ and a film resistivity as low as $1.04 \times 10^{-2} \Omega\text{-cm}$ are achievable.

4. Conclusion

CBD of CdO using three different complexing agents was investigated. XRD revealed that as-grown EA and NH_3 -based films consist of a mixture of cubic CdO_2 , cubic CdO, and monoclinic/hexagonal $\text{Cd}(\text{OH})_2$ while only cubic CdO_2 phase was detected in as-grown MA-based film. Annealing at 400°C in air for 1 h fully transformed as-grown films into cubic CdO. Optical band gap of as-grown EA, NH_3 , and MA-based films are 3.37 eV, 3.40 eV, and 4.64 eV, respectively. Annealed films have optical band gap of 2.53 eV. Both as-grown and annealed films exhibit high transmittance that exceeds 80% in the visible region.

FTIR of as-grown EA-based film showed a broad absorption band around 3300 cm^{-1} , which is assigned to the O–H stretching mode of the hydroxyl group confirming the $\text{Cd}(\text{OH})_2$ phase detected by XRD. Such absorption band disappeared after annealing and did not exist in as-grown MA-based film. RBS observations are consistent with the XRD and FTIR results. Deconvolution of the XPS multiplex of Cd 3d and O 1s peaks of as-grown EA-based film revealed three binding states of CdO_2 , $\text{Cd}(\text{OH})_2$, and CdO; two of which disappeared after annealing which agree with the observations of XRD, FTIR, and RBS. HRTEM showed small variations in film thickness and occasional cracks, due to annealing. The electron diffraction pattern observed confirms the polycrystalline nature of the CdO film. SEM micrographs show high density of cracks in annealed NH_3 -based film. Some pinholes were detected in annealed MA-based films. SEM and Hall measurements revealed that EA-based CdO films are the best candidates for fabricating transparent conducting oxides using CBD, where a carrier density as high as $1.89 \times 10^{20} \text{ cm}^{-3}$ and a film resistivity as low as $1.04 \times 10^{-2} \Omega\text{-cm}$ are achievable.

Acknowledgements

We are grateful to K. Scammon of the Advanced Materials Processing and Analysis Center (AMPAC), University of Central Florida, for his help with the XPS and RBS measurements. We are also grateful to Prof. Aravinda Kar and Mr. G. Lim of College of Optics and Photonics, University of Central Florida, for their help with the Hall measurements, and Prof. Alfons Schulte and his group, especially Mr. Sanghoon Park, of the Department of Physics, University of Central Florida, for their help with the FTIR measurements. This work

was partially supported by USDA award # 58-3148-8-175, Apollo Technologies, Inc. and Florida High Tech. Corridor Council.

References

- [1] G. Kitaev, A. Uritskaya, S. Mokrushin, *Russ. J. Phys. Chem.* 39 (1965) 1101.
- [2] H. Khallaf, I. Oladeji, L. Chow, *Thin Solid Films* 516 (2008) 5967.
- [3] H. Khallaf, I. Oladeji, G. Chai, L. Chow, *Thin Solid Films* 516 (2008) 7306.
- [4] H. Khallaf, G. Chai, O. Lupan, L. Chow, S. Park, A. Schulte, *J. Phys. D: Appl. Phys.* 41 (2008) 185304.
- [5] H. Khallaf, G. Chai, O. Lupan, L. Chow, S. Park, A. Schulte, *Appl. Surf. Sci.* 255 (2009) 4129.
- [6] H. Khallaf, G. Chai, O. Lupan, L. Chow, H. Heinrich, S. Park, A. Schulte, *Phys. Status Solidi (a)* 206 (2009) 256.
- [7] G. Kitaev, T. Terekhova, *Russ. J. Inorg. Chem.* 15 (1970) 25.
- [8] R. Kainthla, D. Pandya, K. Chopra, *J. Electrochem. Soc.* 127 (1980) 277.
- [9] G. Hodes, A. Albu-Yaron, F. Decker, P. Motisuke, *Phys. Rev. B* 36 (1987) 4215.
- [10] J. Gracia-Jiménez, G. Martínez-Montes, R. Silva-González, *J. Electrochem. Soc.* 139 (1992) 2048.
- [11] S. Kale, C. Lokhande, *Mater. Chem. Phys.* 59 (1999) 242.
- [12] M. Najdoski, I. Grozdanov, S. Dey, B. Siracevska, *J. Mater. Chem.* 8 (1998) 2213.
- [13] P. Pramanik, S. Bhattacharya, *Mater. Res. Bull.* 24 (1989) 945.
- [14] B. Pejova, M. Najdoski, I. Grozdanov, S. Dey, *J. Mater. Chem.* 9 (1999) 2889.
- [15] I. Oladeji, L. Chow, *Thin Solid Films* 339 (1999) 148.
- [16] P. O'Brien, D. Otway, D. Smyth-Boyle, *Thin Solid Films* 361–362 (2000) 17.
- [17] J. Doña, J. Herrero, *J. Electrochem. Soc.* 141 (1994) 205.
- [18] I. Ndukwe, *Sol. Energy Mater. Sol. Cells* 40 (1996) 123.
- [19] P. Pramanik, S. Biswas, *J. Electrochem. Soc.* 133 (1986) 350.
- [20] J. Doña, J. Herrero, *J. Electrochem. Soc.* 142 (1995) 764.
- [21] C. Estrada, P. Nair, M. Nair, R. Zingaro, E. Meyers, *J. Electrochem. Soc.* 141 (1994) 802.
- [22] A. Chaparro, M. Martínez, C. Guillén, R. Bayón, M. Gutiérrez, J. Herrero, *Thin Solid Films* 361–362 (2000) 177.
- [23] H. Khallaf, G. Chai, O. Lupan, H. Heinrich, S. Park, A. Schulte, L. Chow, *J. Phys. D: Appl. Phys.* 42 (2009) 135304.
- [24] T. Saeed, P. O'Brien, *Thin Solid Films* 271 (1995) 35.
- [25] M. Ortega-López, A. Avila-García, M. Albor-Aguilera, V. Resendiz, *Mater. Res. Bull.* 38 (2003) 1241.
- [26] A. Ennaoui, M. Weber, R. Scheer, H. Lewerenz, *Sol. Energy Mater. Sol. Cells* 54 (1998) 277.
- [27] T. Subramanyam, B. Krishna, S. Uthanna, B. Naidu, P. Reddy, *Vacuum* 48 (1997) 565.
- [28] X. Li, T. Gessert, T. Coutts, *Appl. Surf. Sci.* 223 (2004) 138.
- [29] D. Ellis, S. Irvine, *J. Mater. Sci.: Mater. Electron.* 15 (2004) 369.
- [30] A. Dakhel, *J. Alloys Compd.* 475 (2009) 51.
- [31] J. Chang, R. Mane, D. Ham, W. Lee, B. Cho, J. Lee, S. Han, *Electrochem. Acta* 53 (2007) 695.
- [32] R. Gupta, K. Ghosh, R. Patel, S. Mishra, P. Kahol, *Mater. Lett.* 62 (2008) 4103.
- [33] H. Ali, H. Mohamed, M. Wakkad, M. Hasaneen, *J. Appl. Phys.* 48 (2009) 041101.
- [34] R. Salunkhe, D. Dhawale, D. Dubal, C. Lokhande, *Sens. Actuators B* 140 (2009) 86.
- [35] S. Aksoy, Y. Caglar, S. Ilican, M. Caglar, *Int. J. Hydrogen Energy* 34 (2009) 5191.
- [36] B. Saha, R. Thapa, K. Chattopadhyay, *Sol. Energy Mater. Sol. Cells* 92 (2008) 1077.
- [37] R. Salunkhe, D. Dhawale, T. Gujar, C. Lokhande, *Mater. Res. Bull.* 44 (2009) 364.
- [38] L. de León-Gutiérrez, J. Cayente-Romero, J. Peza-Tapia, E. Barrera-Calva, J. Martínez-Flores, M. Ortega-López, *Mater. Lett.* 60 (2006) 3866.
- [39] M. Ocampo, A. Fernandez, P. Sebastian, *Semicond. Sci. Technol.* 8 (1993) 750.
- [40] J. Pankove, *Optical Processes in Semiconductors*, Dover Publications, New York, 1971.
- [41] Joint Committee on Powder Diffraction Standards, *Powder Diffraction File No. 075-0591*.
- [42] Joint Committee on Powder Diffraction Standards, *Powder Diffraction File No. 084-1767*.
- [43] Joint Committee on Powder Diffraction Standards, *Powder Diffraction File No. 073-0969*.
- [44] Joint Committee on Powder Diffraction Standards, *Powder Diffraction File No. 078-1125*.
- [45] Joint Committee on Powder Diffraction Standards, *Powder Diffraction File No. 075-0592*.
- [46] M. Najdoski, I. Grozdanov, B. Minceva-Sukarova, *J. Mater. Chem.* 6 (1996) 761.
- [47] T. Gujar, V. Shinde, W. Kim, K. Jung, C. Lokhande, O. Joo, *Appl. Surf. Sci.* 254 (2008) 3813.
- [48] P. Pascuta, R. Lungu, I. Ardelean, *J. Mater. Sci.: Mater. Electron.* 21 (2010) 548.
- [49] L. Doolittle, *Nucl. Instrum. Methods B* 15 (1986) 227.
- [50] J. Moulder, W. Stickle, P. Sobol, K. Bomben, in: J. Chastain (Ed.), *Handbook of X-ray Photoelectron Spectroscopy*, Perkin-Elmer Corporation, Minnesota, 1992.
- [51] J. Dupin, D. Gonbeau, P. Vinatier, A. Levasseur, *Phys. Chem. Chem. Phys.* 2 (2000) 1319.